Science Advances
AAAS

advances.sciencemag.org/cgi/content/full/5/2/eaau7378/DC1

Supplementary Materials for

Internal ion-gated organic electrochemical transistor: A building block for integrated bioelectronics

George D. Spyropoulos, Jennifer N. Gelinas*, Dion Khodagholy*

*Corresponding author. Email: jng2146@cumc.columbia.edu (J.N.G.); dion@ee.columbia.edu (D.K.)

Published 27 February 2019, *Sci. Adv.* **5**, eaau7378 (2019)
DOI: 10.1126/sciadv.aau7378

This PDF file includes:

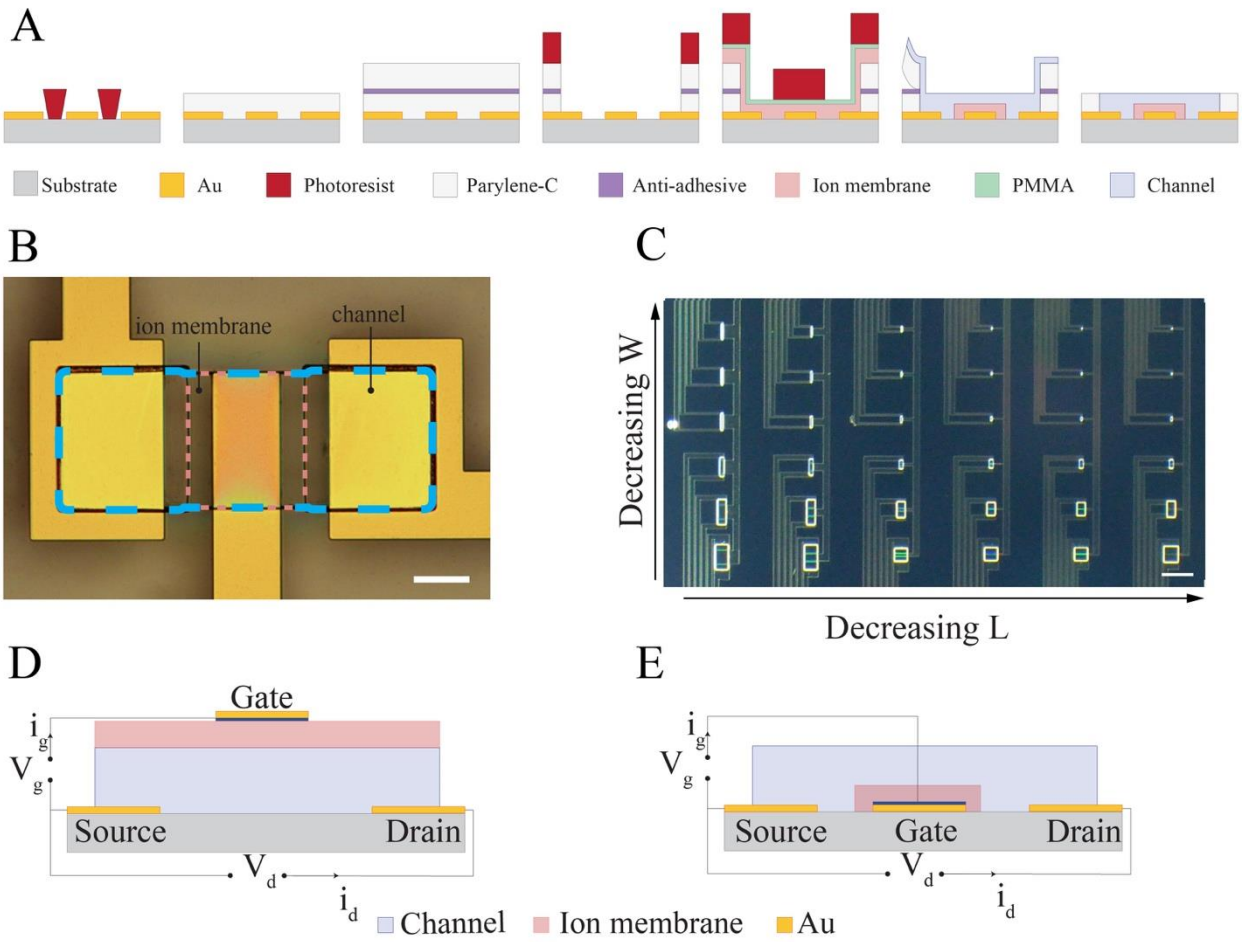

Fig. S1. Fabrication process and IGT architecture. (**A**) IGT fabrication process; i) patterning of Au electrodes and interconnects via photolithography and lift-off process; ii) deposition of parylene-C layer; iii) coating of an anti-adhesive layer and deposition of sacrificial parylene-C layer; iv) opening of the transistor channel areas via successive photolithography and plasma etching steps; v) coating of ion membrane and PMMA protective layer, then patterning via successive photolithography and plasma etching steps; vi) removal of PMMA layer with acetone, coating of channel, and peeling-off the sacrificial parylene-C layer; vii) final IGT. (**B**) Optical micrograph displaying the top view of an IGT with L = 60 µm and W = 50 µm. Scale bar, 20µm. (**C**) Microfabricated 6 × 6 IGT array used for characterizing effect of channel dimensions. Channel L and W decrease logarithmically from 500 µm to 5 µm. Scale bar 1 mm. (**D**-**E**) Schematic cross-section illustration of IGTs with top and bottom gate locations. These architectures have identical electrical characteristics as shown by the overlaid circuit diagrams, but the majority of the experiments were conducted using the architecture in E) based on fabrication process shown in A).

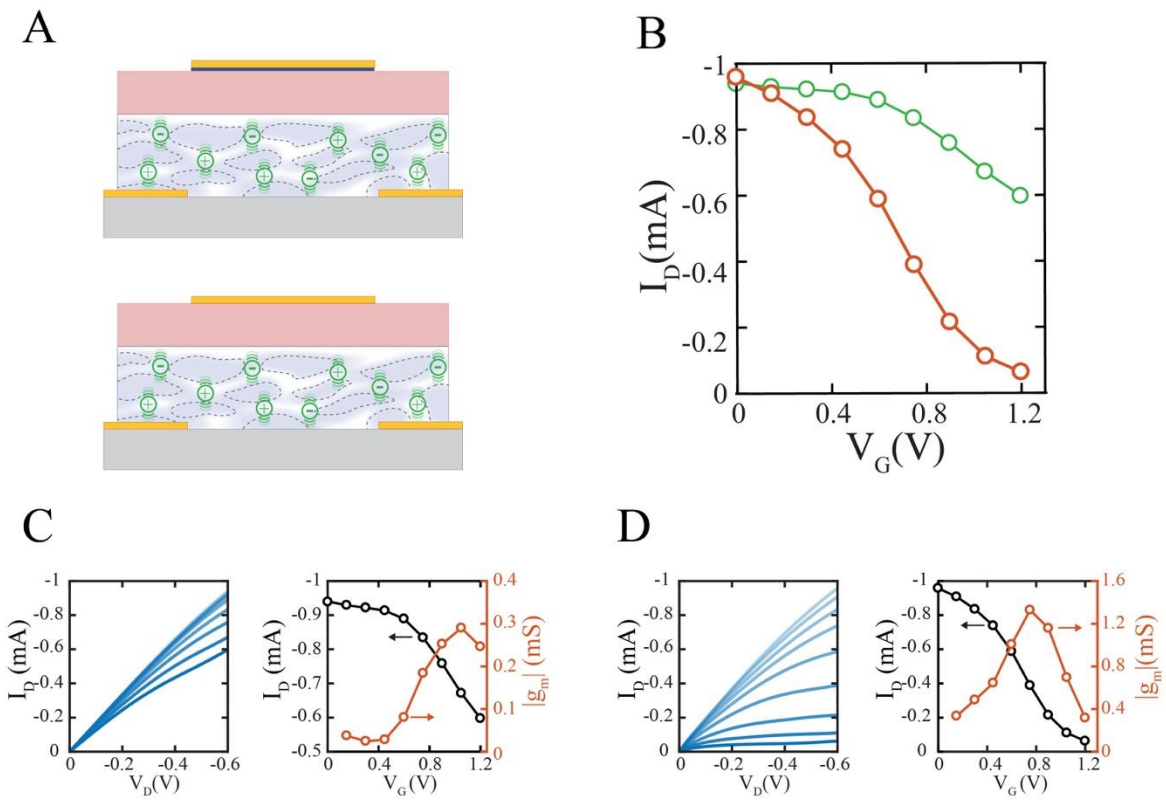

Fig. S2. PEDOT:PSS reduces the chitosan-Au electrochemical impedance at the IGT gate. (**A**) Schematic cross-section illustration of IGTs with (top) and without (bottom) PEDOT:PSS in the ion membrane. (**B**) Transfer curves for V_D = -0.6 V (L = 5 mm, W = 10 mm) with chitosan (CS; green) and successively coated PEDOT:PSS/CS (orange) forming the ion membrane. Corresponding output characteristics, transfer curves and transconductance (varying V_G from 0 V (top curve) to +1.2 V (bottom curve)) for CS-only IGT are shown in (**C**) and for PEDOT:PSS/CS IGT in (**D**).

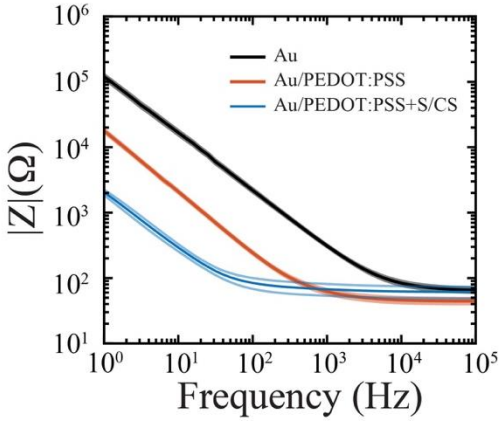

Fig. S3. Comparison of electrochemical impedance of different material interfaces. Electrochemical impedance spectroscopy for Au (black), Au/PEDOT:PSS (red) and Au/PEDOT:PSS+D-Sorbitol(S)/CS (blue) 4mm^2 electrodes. Solid lines show the mean values derived from 15 measurements (3 measurements for 5 different electrodes) per interface. Semitransparent lines show the corresponding mean value ± standard deviation. The film thickness of PEDOT:PSS and PEDOT:PSS+S was tuned to result in equal resistance.

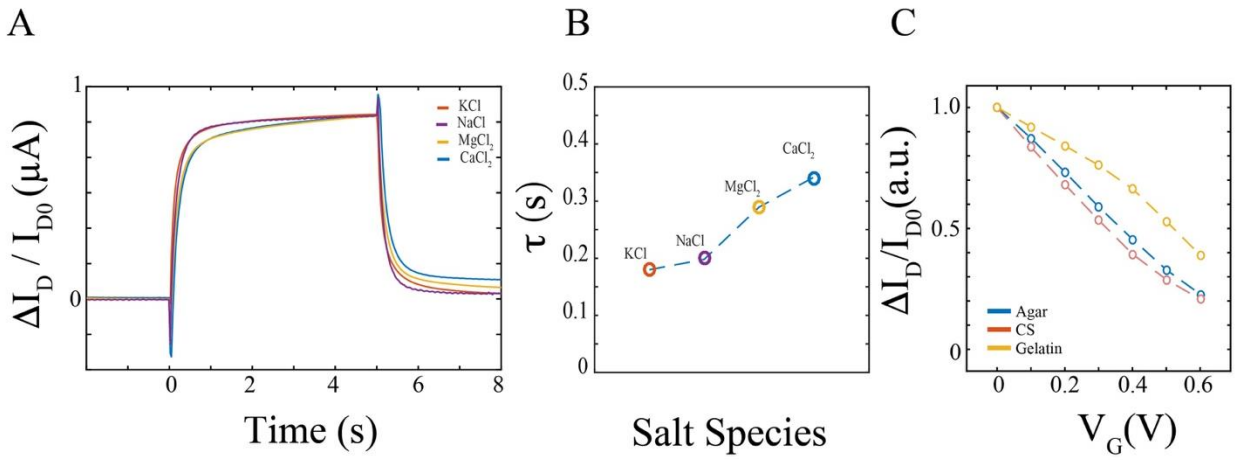

Fig. S4. Comparison of ion species and ion membrane material on modulation magnitude and rise time of IGTs. (**A**) Temporal response of the drain current (I_D) of an IGT device with L = 1.5 mm and W = 3 mm using a channel containing different ion species (V_{DS} = -0.6, V_{GS} pulse amplitude = 0.4 V). (**B**) Corresponding time constants derived from exponential fit of the IGT drain current for each ion species in A); W, L = 2.5 mm, 2.5 mm. (**C**) Normalized response of the drain current (I_D) of IGTs employing gelatin, agar and chitosan as the ion-membrane material (V_{DS} = -0.6, L = 5 mm, W = 10 mm).

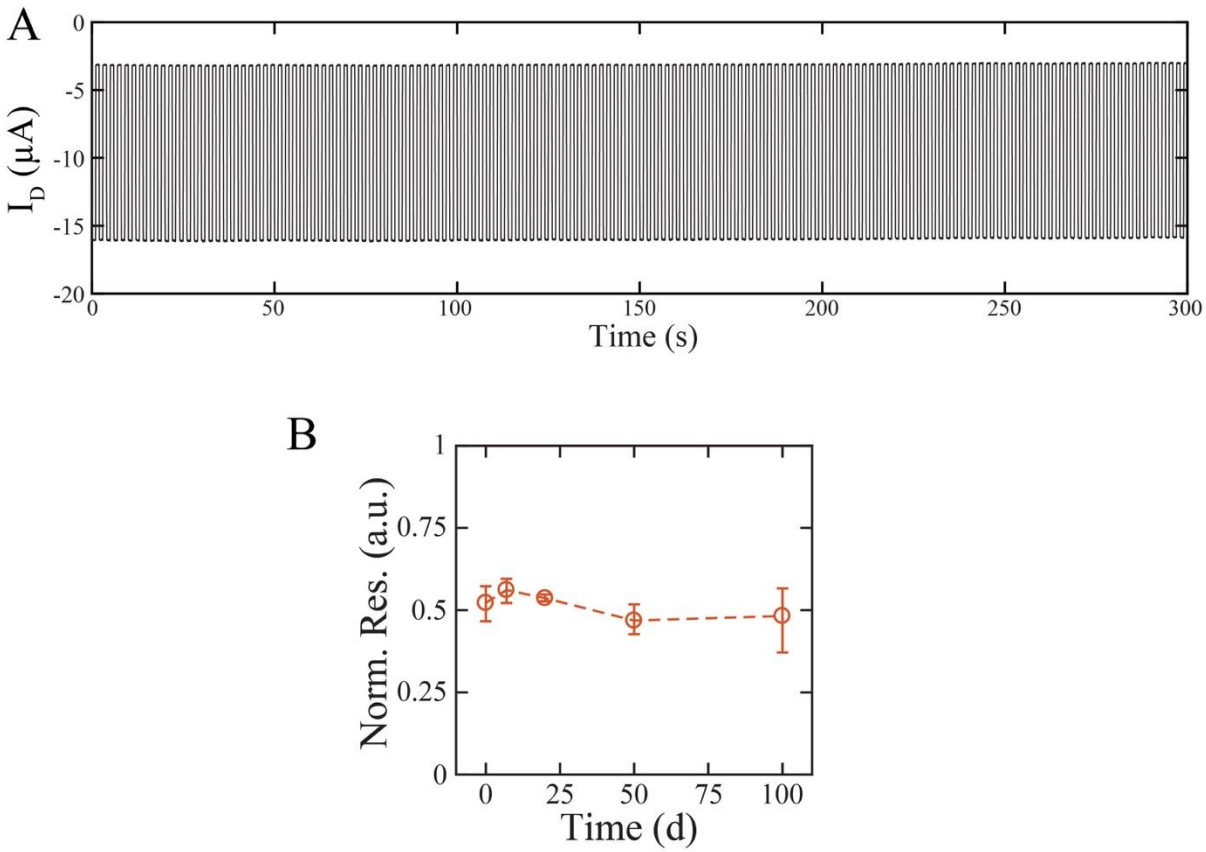

Fig. S5. Internal mobile ions enable stable operation over time without a decrement in speed or significant drift in drain current. (**A**) Temporal response of the drain current (I_D) of an IGT device under continuous long-term operation with pulsed gate voltage (V_D = -0.4 and V_G = 0 to 0.4; W, L = 250, 5 µm). (**B**) Normalized response ((I_D –I_{D0})/ I_{D0} of IGT over a time period of 100 days without hydration for ΔV_G = 0.6 V, V_D = -0.6V. I_{D0} denotes baseline drain current. Each data point represents the average value of 3 IGT devices with L = 5 mm, W = 10 mm. Error bars represent the maximum and minimum value for each data point.

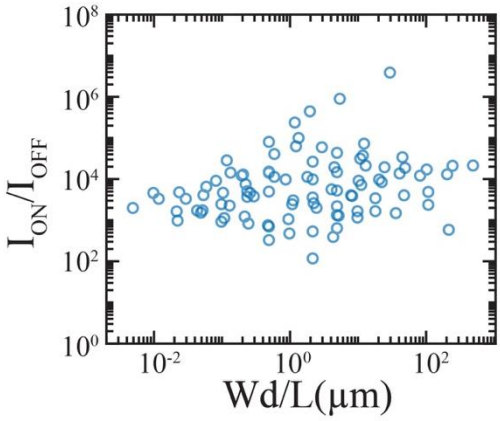

Fig. S6. Effect of channel geometry on IGT I_{on}/I_{off}. On/Off current ratio as a function of channel geometry. The I_{on}/I_{off} was calculated for a 6 × 6 array of IGTs with logarithmically increasing channel length and width; V_D = -0.15 V and V_{GS} = 0.7 V.

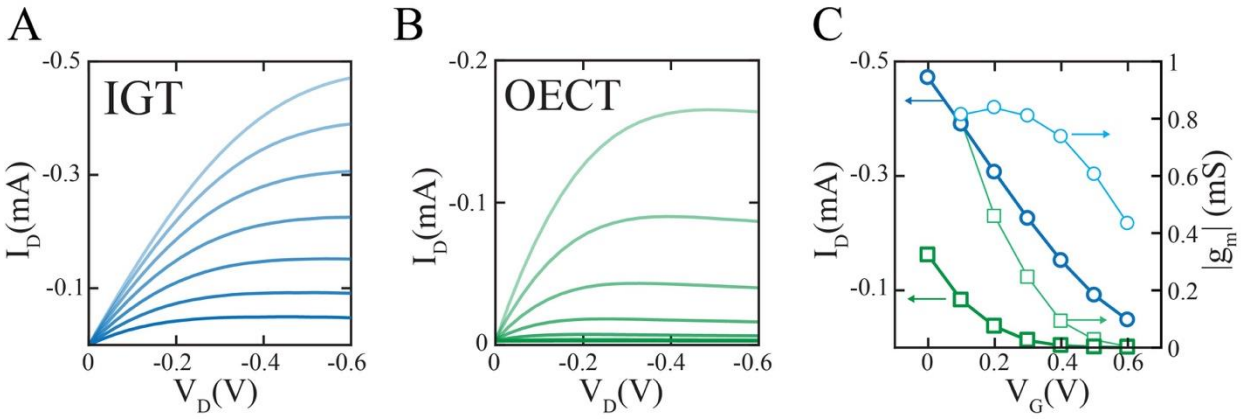

Fig. S7. Output characteristics of IGT and OECT devices with identical geometry. I_D-V_D characteristics of IGT (**A**) and OECT (**B**) device with L = 30 μm and W = 12 μm. V_G varies from 0 V (top curve) to +0.6 V (bottom curve) with a step of +0.1 V. (**C**) Corresponding transfer curves and transconductance for IGT (blue circles and light blue circles) and OECT (green squares and light green squares, V_{DS}= -0.6 V).

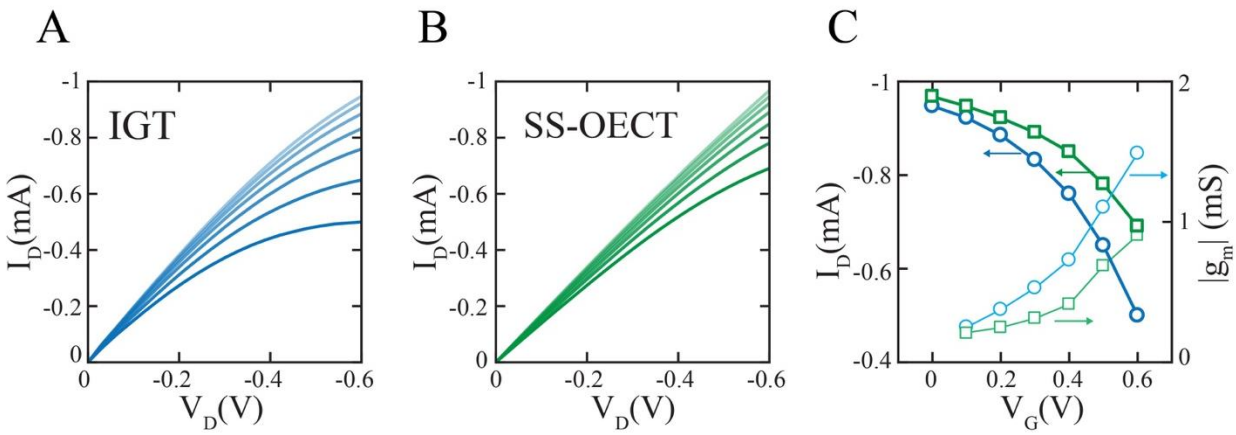

Fig. S8. Output characteristics of IGT and SS-OECT devices with identical geometry. I_D-V_D characteristics of IGT (**A**) and SS-OECT (**B**) device with L = 5 mm and W = 10 mm. V_G varies from 0 V (top curve) to +0.6 V (bottom curve) with a step of +0.1 V. (**C**) Corresponding transfer curves and transconductance for IGT (blue circles and light blue circles) and SS-OECT (green squares and light green squares, V_{DS}= -0.6 V).